Research Square

Preprints are preliminary reports that have not undergone peer review.
They should not be considered conclusive, used to inform clinical practice,
or referenced by the media as validated information.

Enhancing solubility and antibacterial properties of Cefpodoxime Proxetil by using rice husk derived nanocellulose as a drug carrier: A novel approach

Mukta Rajotia
Banasthali Vidyapith
Subrata Panda
pandas.cer@iitbhu.ac.in
Indian Institute of Technology (BHU) https://orcid.org/0000-0002-6441-5729
Vivek Kumar Saroj
Indian Institute of Technology (BHU)

Research Article

Keywords: Rice husk, Nanocellulose, Drug carrier, Cefpodoxime Proxetil, Bioavailability

Posted Date: June 25th, 2026

DOI: https://doi.org/10.21203/rs.3.rs-7496846/v1

License: This work is licensed under a Creative Commons Attribution 4.0 International License.
Read Full License

Additional Declarations: The authors declare no competing interests.

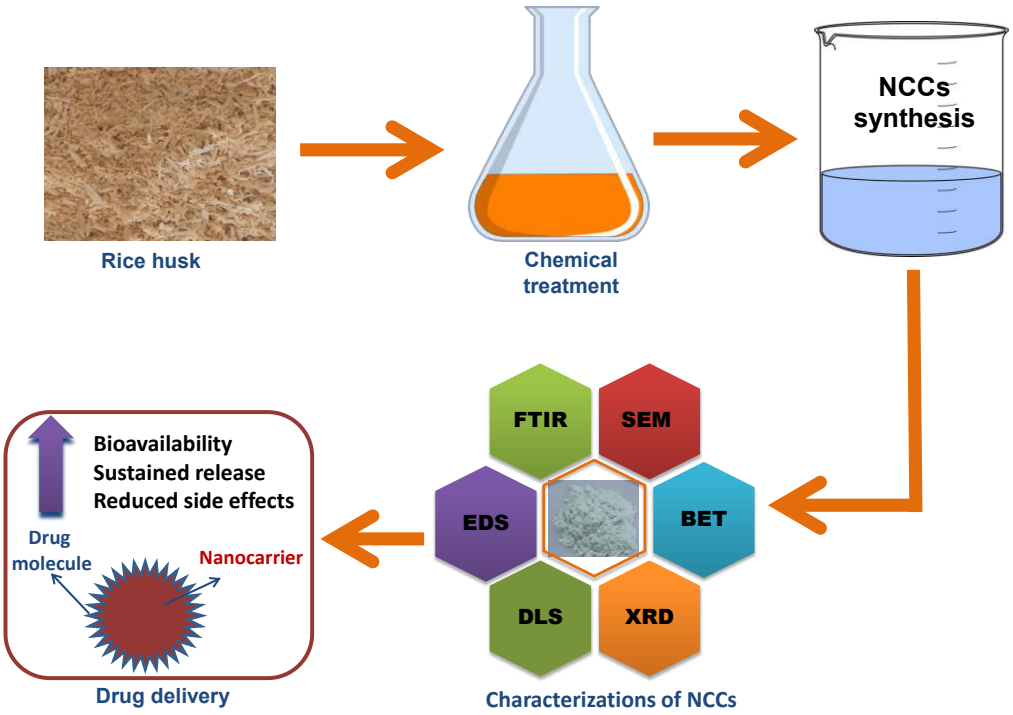
Enhancing solubility and antibacterial properties of Cefpodoxime Proxetil by using rice husk derived nanocellulose as a drug carrier: A novel approach

Mukta Rajotia[1], Bechan Sharma[2], Vivek Kumar Saroj[3], Priya Singh[4], Sanjeev Kumar Mahto[4], Subrata Panda[3*]

[1] Department of Chemistry, Banasthali Vidyapith, Niwai 304022, Rajasthan, India
[2] Department of Biochemistry, University of Allahabad, Allahabad 211001, Uttar Pradesh, India
[3] Department of Ceramic Engineering, Indian Institute of Technology (BHU), Varanasi 221005, Uttar Pradesh, India
[4] School of Biomedical Engineering, Indian Institute of Technology (BHU), Varanasi 221005, Uttar Pradesh, India

* Corresponding Author email: pandas.cer@iitbhu.ac.in

Graphical Abstract:



Abstract:

The issue of poor aqueous solubility of drugs is increasingly prominent in the formulation and development of drug delivery systems. In this study, we address such issues by developing nanocellulose crystals (NCCs) as a potential drug delivery carrier to enhance the solubility of poor water soluble drugs. The NCCs are extracted from a rice husk biowaste. Structural analysis of the NCCs clearly substantiates its nanometric size, high specific surface area, uniform pore size distribution and the presence of functional groups further qualifies its capability of facilitating drug delivery. Thus, a cefpodoxime proxetil (CP) prodrug is loaded in the NCCs and prepared a CP-NCCs formulation. The encapsulation efficiency, release kinetics, and stability of the CP-NCCs formulation were thoroughly evaluated, indicating an overall improvement of drug delivery performance. Moreover, zone of inhibition via disc diffusion study clearly indicates excellence antibacterial property of the CP-NCCs formulation. This research not only highlights the promising capabilities of rice husk derived nanocellulose for drug delivery applications but also demonstrated the feasibility of nanocellulose in enhancing the solubility and consequently, the potential bioavailability of poorly soluble drugs.

Key words: Rice husk, Nanocellulose, Drug carrier, Cefpodoxime Proxetil, Bioavailability

Highlights:

- Extraction of nanocellulose crystals from the rice husk by economically viable route
- Nanocellulose crystals showed excellence drug delivery efficacy of cefpodoxime proxitel
- Utilization of biowaste and contribution to the sustainability and circular economy

1. Introduction

Cellulose is the most abundant biopolymer on earth. The global annual output of cellulose in all over the world is about 75 to 100 billion metric tonnes . It can be produced by plants, organisms such as fungi, bacteria, tunicates and amoeba. Cellulose production from different organisms is much smaller as compared to plants ,. In previous research works, the nanocellulose crystals (NCCs) have been successfully produced from various lignocellulosic biomasses such as corn cob, rice straw etc. , . According to some reports, the earth's total living biomass is approximately 550–560 billion tonnes with an annual primary production of biomass exceeding 100 billion tonnes . Globally, four main agricultural crops in terms of both harvested area and output are rice, maize, wheat, and sugarcane. The annual production of biomass from rice, maize, wheat, and sugarcane crops' yields have been reported to be about 904.92 million tones, 2723.70 million tones, 681.92 million tons, and 1048.0 million tons of dry biomass, respectively . It is estimated that carbon emission from biomass burning account for roughly 20% to 33%, which is one fifth to one third of the carbon released from emission of fossil fuel. This biomass needs to be effectively and properly utilized for production of fuels and chemicals . Rice, the most abundant cereal crop globally, generates a significant volume of rice husk (RH), accounting for approximately 45% of the residue produced in rice cultivation. However, utilizing RH poses challenges due to its limited nutritional value compared to other cereal straws and its tendency to produce excessive ash when used as a fuel source. Given these concerns, there is a pressing need to explore alternative ways to make use of RH, especially considering environmental implications. With its composition comprising cellulose (38.3%), hemicellulose (31.6%), lignin (11.8%), and silica (18.3%), RH stands out as the most abundant source of cellulose among agricultural crop residues worldwide .

Cellulose nanofibers or particles can be produced by chemical or mechanical processes of biomasses such as acid hydrolysis. During acid treatment, the glycosidicbonds undergo hydrolytic cleavage mainly in the amorphous regions of the cellulose leading to first degradation of amorphous region; the releasing crystalline regions are retained . These cellulose solids, known as cellulose crystals, are rod-shaped and highly crystalline. The initial successful creation of cellulose nanocrystals occurred in 1947 when Nickerson and Habrle hydrolyzed cellulose using hydrochloric acid and sulfuric acid. Subsequently, in 1953, Mukherjee and Woods demonstrated through X-ray technology and electron microscopy that the needle-like particles obtained from sulfuric acid hydrolysis were indeed of nanometer size. They also confirmed that these particles maintained the crystal structure of raw cellulose , .

Cellulose has wide applications in veterinary foods, wood and paper industry, fibers and clothes, cleaning oil spills, cosmetics, medical and pharmaceutical industries . In its nanocrystalline form, it has a very high tensile strength (7 times that of steel), electrically conductive, light weight and highly absorbent when used as a basis for aero gels . This novel material has the potential to substitute certain petrochemical-based products and is highly probable to be more cost-effective than many other types of high-performance nanomaterials. The first commercial product derived from cellulose was made from camphor and nitrocellulose by the Hyatt Manufacturing Company in 1870 .

Due to hydrophobic nature and better bioavailability, the NCCs can be used in drug delivery system to solubilize poorly water-soluble drugs and they can provide prolonged release into the systems. Cellulosic materials, which contain hydroxyl groups, are capable of reacting with the various hydrophobic groups to form ester bonds, creating amphiphilic polymers. These covalent bonds between cellulose and hydrophobic groups can be employed in biomedical fields, particularly for controlled drug release applications. -.Cellulose nanoparticles have been used as a vehicle for drugs such as curcumin, phenytoin, and moxifloxacin, which present problems of bioavailability because of their low or non-existent solubility in water -. Cefpodoxime Proxetil (CP) is an orally administrated, extended spectrum, semi synthetic, and β-lactum antibiotic of the cephalosporin class. This prodrug undergoes de-esterification *in vivo* to form cefpodoxime, facilitated by esterase enzymes in the gastrointestinal wall. Absolute bioavailability of CP administrated as a 130 mg tablet in human is only about 50 % -. The limited bioavailability of CP primarily results from the breakdown of its ester side chain by cholinesterase in the intestinal lumen. Its poor solubility in water (400 μg/ml) also contributes to its low bioavailability because dissolution is a critical limiting factor for the intestinal absorption of drugs that do not dissolve well. CP is classified as a biopharmaceutical classification system (BCS) class IV drug, with a logP value of 0.99 and a melting point of 84 °C -.

In this context, this study primarily focuses on the sustainable and ecofriendly utilization of rice husk derived NCCs a drug carrier to improve stability and solubility of cefpodoxime proxetil in phosphate buffered saline (PBS). The use of NCCs as a drug carrier depends on formulation and development of drug delivery system. The NCCs extracted from the rice husk via a simple chemical processing route were applied for studying their drug carrying and releasing abilities in the PBS solution. Both studies demonstrated excellent drug carrying properties. This study realizes the utilization of rice husk not only for reducing biowaste but also for aligning with the principle of a circular and sustainable bio-economy.

2. Experimental Details

2.1 Materials and Methods

Rice husk was collected from the Amazon online platform and other chemicals such as sodium hydroxide (97%), sulfuric acid (98%) were purchased from Merck Life Science private Limited (Mumbai), glacial acetic acid (98%), hydrogen peroxide (30%, v/v), filter paper (125 mm) was purchased from M. K enterprises, U.P. All chemicals were of analytical grade. Cefpodoxime Proxetil prodrug was supplied as a gift sample.

2.1.1 Synthesis of NCCs from RH

Collected RH was washed several times with distilled water to remove all dust particles and then oven dried in an electric oven at 80 °C for 24 h. The process of cellulose extraction from the RH was conducted by applying three steps. Firstly, the RH was treated with 5N H_2SO_4 at 90 ℃ for 2 h to hydrolyze hemicellulose and to remove some organic impurities. After acid hydrolysis,the residue was washed 3-4 times with distilled water to remove sulphate group present in it. Secondly, the acid hydrolyzed RH was treated with sodium hydroxide for 3 h at 110 ℃ with continious stirring and then autoclaved at 121 ℃ for 45 min. This steam explosion process was repeated twice to maximize the delignification efficancy and ease of removal of non-cellulosic component such as hemicellulose, pectin, and waxy materials. After the steam explosion, the residue was washed 3-4 times with distilled water to remove some alkali soluble impurities. Finally, the alkali treated RH residue was bleached with 1:1 solution of hydrogen peroxide (30%, v/v) and glacial acetic acid at 80 °C for 8 h with continious stirring to obtain pure white fibers. The moist product was then oven dried and stored in an airtight container. The obtained white powder was then charcaterized by using the spectroscopic techniques for structural analysis in details.

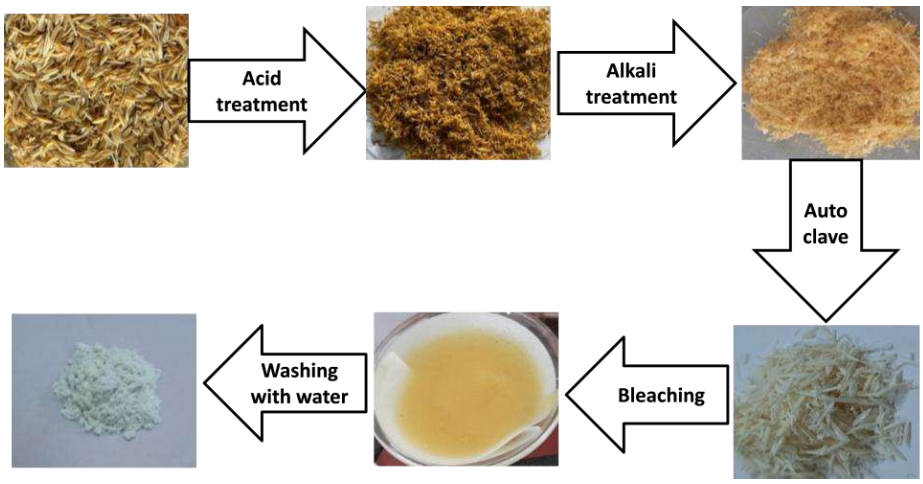


Fig. 1. Schematic represeantation of preparation of nanocellulose crystals from the rice husk biowaste.

2.1.2 Evaluation of drug loading on NCCs

The adsorption study of CP on NCCs was conducted isothermally at 30 ℃. The procedure was as follows: a saturated solution of the pure drug was prepared in an Erlenmeyer flask using a 1:1 mixture of ethanol and dichloromethane (DCM) and a specific amount of NCCs was added to this solution. The flask was then placed on a magnetic shaker for continuous shaking for 24 h. During this process, the system was maintained at a temperature of 30 °C. The NCCs were then separated from the solution via centrifugation. After centrifugation, the NCCs were separated from the sample by simple filtration method. The solid part was considered as drug loaded carrier and named as CP-NCCs. The supenatent was used to find the concentration of drug in the solution. The initial concentration of drug in the solution before loading and after loading were determined using a Jasco V-770 UV/VIS Spectrophotometer at the maximum wavelength of 263 nm. A calibration curve was plotted with known concentration of drug in 1:1 mixture of DCM and ethanol for quantitative analysis of drug in various samples. The amount of CP adsorbed by the NCCs was calculated by using the following equation (1) .

$$\text{Total amount of drug adsorbed (\%)} = \frac{Co-Ce}{Co} \times 100 \quad (1)$$

Where, C_0 and C_e are the concentration of drug before and after adsorbed respectively.

2.1.3 Drug release study in PBS solution

For drug release study, a specific quantity of drug-loaded nanocellulose particles, referred to as CP-NCCs, were sequentially placed into 50 ml of PBS solution (pH 1.2) in an incubator set at 37 °C with continuous shaking at 200 rpm. The pH 1.2 for the PBS solution was selected to test its release study because CP is a prodrug that is designed to be converted into its active form cefpodoxime, in the body in an acidic environment. The acidic environment of the stomach is crucial for the hydrolysis of the prodrug. Evaluating drug release at pH 1.2 helps in understanding how well the prodrug releases the active drug under these conditions. At designated time intervals, samples were withdrawn from the solutions one by one, and the concentration of released drug over time was determined using a UV-Vis spectrometer. The drug release experiment was determined by following the established protocols from previous studies .

2.1.4 Antibacterial tests

For antibacterial test, we have used Gram positive bacteria, *B. subtilis* and Gram negative as well as CP sensitive *E. coli* strain. We resuscitated the lyophilized cells on nutrient broth and culture on nutrient agar medium. For antibiotic susceptibility assay: The National Committee for Clinical Laboratory Standards (NCCLS) guidelines were followed to perform the antibiotic susceptibility assay on agar media. The bacterial solution (200 µl) was spread on the solidified agar and plated with the help of L-shape glass rod. A small well was cut in agar plates for the same. The solid sample (0.4 mg) was added into the well. The CP antibiotic alone named as CP1 and in combination with NCCs named as NCP1 were used. The NCCs alone were also employed and named as NCC1. All the plates were incubated at 37 ℃, and after 24 h of an interval zone of inhibition (ZOI) was measured for all the plates.

2.2 Materials Characterization

The yield of NCCs was calculated by using the following equation (2) .

$$Yield = \frac{W_f}{Wi} \times 100 \quad (2)$$

Where, W_f and W_i denotes the final weight of product and the initial weight of the RH, respectively.

Fourier Transform Infrared (FTIR) spectrophotometer (THERMO Electron Scientific Instruments LLC, Nicolet- iS5) was used to find the functional groups present in the sudiews samples. The spectral data were collected in transmittance mode with an accumulation of 128 scans at a resolution of 4.00 cm^{-1} from 550 cm^{-1} to 4000 cm^{-1} range. The morphological characterizations of all the samples were done by High Resolution Scanning Electron Microscope-Energy-Dispersive X-ray spectrometry (EVO-SEM MA15/18, Carl Zeiss). To conduct the analysis, the sample was coated with gold nanoparticles to improve conductivity. The average particle size and particle size distribution of NCCs was done at Malvern Panalytical, Zetasizer Ver.7.13 by using Dynamic Light Scattering (DLS) Instrument. The test was carried out at room temperature, viscosity 0.8872 cP, count rate (kcps) 128.3, and material refractive index (RI) 1.59.

The crystallinity analyses for the samples were carried out using an X-ray Diffractometer (RIGAKU Corporation, Rigaku Miniflex 600 Desktop X-ray Diffraction System). The crystanillity index of all samples were identified by utilizing the following equation (3) .

$$\text{Crystanillity Index (CI\%)} = \frac{Area\ of\ all\ crystalline\ peaks}{Area\ of\ all\ crystalline\ and\ amorphous\ peaks} \times 100 \quad (3)$$

The surface-related properties like pore size distribution, total pore volume, and average pore size of the nanoparticles was calculated by using Surface Area Measurement Facility (BELLSORP MAX II & BELCAT-II Microtrac BEL Corp.). All the characterizations were done with the powder samples.

3. Results and discussion

3.1 Structural analysis of NCCs

The total yield of the NCCs extracted from the RH was about 20%. Similar studies have shown that cellulose nanoparticles yield from the RH ranges between 19% and 26% . The functional groups present in the rice husk and the extracted NCCs were analyzed by using FTIR and interpreted on the bases of observed peaks corresponding to functional group. **Fig. 2** shows the spectra highlighting various spectral bands identified from the results. The dominant broad absorption peak at 3330 cm^{-1} is associated with the –OH stretching vibration, indicative of either cellulose fibers or water content. The absorption peak from near 2800 -2920 cm^{-1} corresponds to the C-H stretching in cellulose fibers, which decreases in intensity and becomes broader in the case of NCCs spectra.

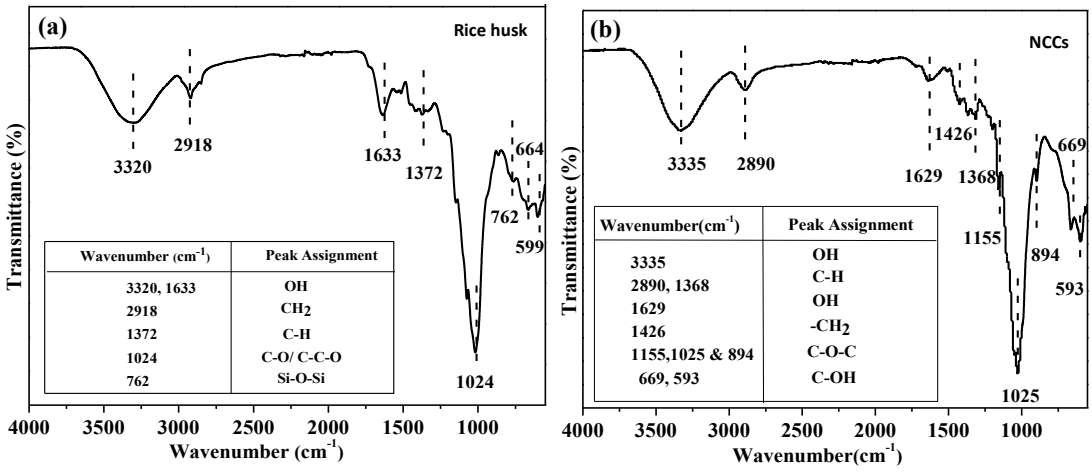


Fig. 2. FTIR spectra of (a) the RH and (b) the extracted NCCs.

The peak at 1640 cm^{-1} is presented to -OH vibration, the -OH peaks are linked to the stretching of hydrogen bonds in the cellulose structure. A smaller band observed in RH at 1732 cm^{-1}, corresponded to acetyl and uronic ester groups present in hemicellulose or the ester linkages of carboxylic groups from ferulic and p-coumaric acids in lignin and hemicellulose, was absent in the NCCs spectra. This absence confirmed the removal of lignin and hemicellulose components from the RH. Additionally, the peak at 1426 cm^{-1} represented the -CH_2 functional group of cellulose, while the peak at 1368 cm^{-1} originates from the C-H group of cellulose. Notably, the prominent peaks for cellulose at 1155

cm^{-1}, 1025 cm^{-1}, and 894 cm^{-1}were associated with the C-O-C functional groups, indicating the glycosidic linkage present in cellulose. The peaks at 1368 cm^{-1} and 1426 cm^{-1}were characteristic peaks of pure cellulose-. The spectra peaks at 1024 cm^{-1} in the RH showed Si-O-Si bonding and C-O bonding, peaks at 762 cm^{-1} and below this range were due to asymmetric stretching of bonding oxygen present in the RH silica, absence or decrease in intensity of these peaks in the NCCs confirmed the removal of silica and high purity of cellulose particles , .

Surface morphology of the NCCs was analyzed by HR-SEM at different magnification as shown in **Fig. 3**. Visually, it was evident that nano-sized particles were prepared with irregular shape and size. According to the SEM micrographs, the cellulose nanoparticles appeared predominantly spherical in shape and were observed to be agglomerated into various sizes after the drying process.

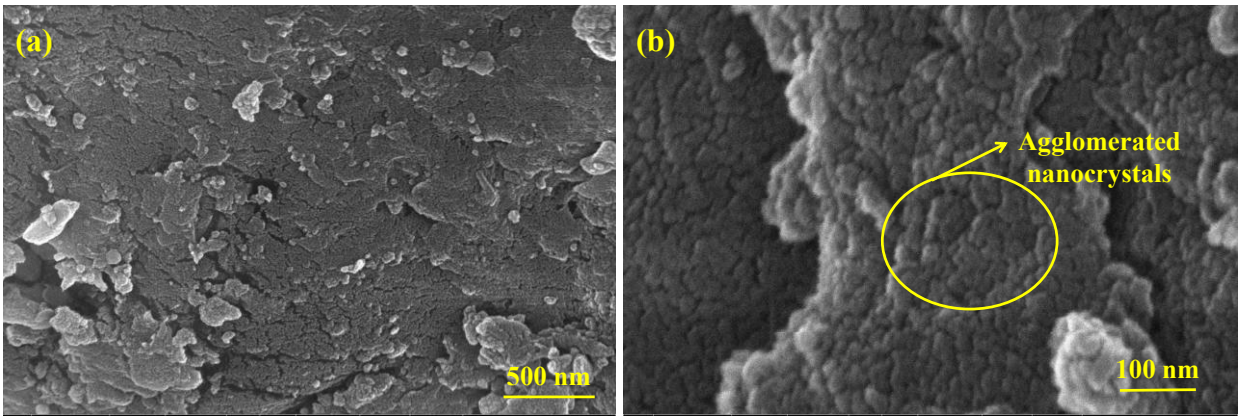


Fig. 3. SEM micrographs of NCCs particles at (a) lower magnification and (b) higher magnification.

The particle size distribution and average particle size of the NCCs particles were measured by using dynamic light scattering (DLS) and shown in **Fig. 4**. This technique provided the distribution and average size of the NCCs, as well as the polydispersity index (PDI), which indicates the uniformity of the particles in suspension. Typically, a PDI value below 0.1 suggested a monodisperse distribution, characterized by uniform peaks. The PDI of the NCCs was reported as 0.560. The particle size ranged from 50 nm to 200 nm, with an average size of 166.1 nm, confirming the nanocrystalline features and a uniform distribution of the NCCs particles.

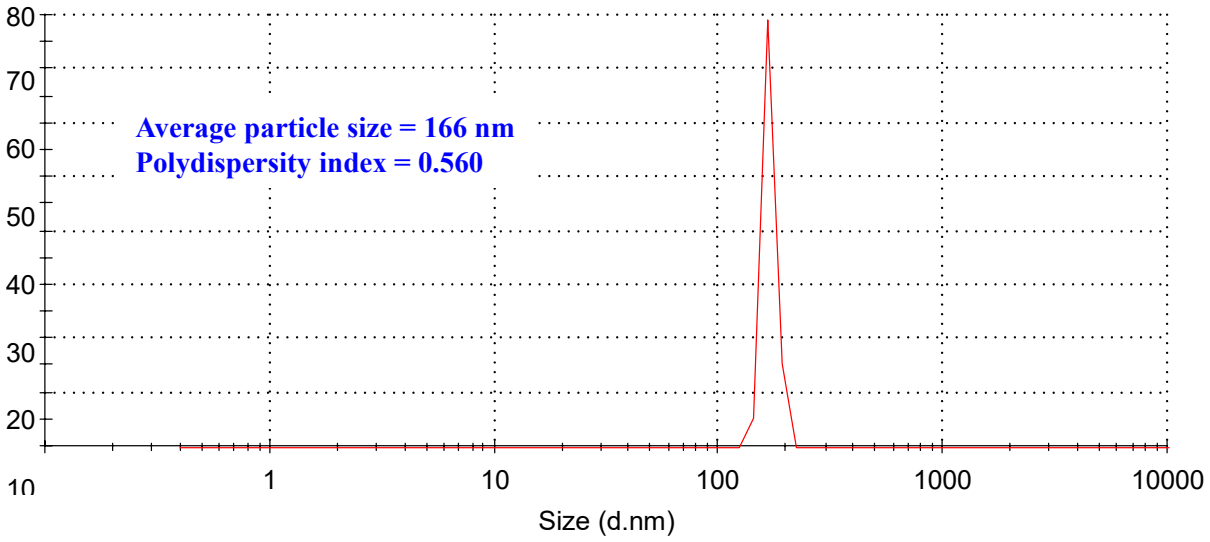


Fig. 4. Particle size distribution of the NCCs particles.

The XRD analysis of the RH and NCCs, shown in **Fig. 5**, revealed the crystalline peaks across a scan range of 2θ = 10 to 80°. The crystallinity index was derived by using equation (3). Initially, the crystallinity for the NCCs was determined by calculating both the crystalline peak area and the total area for all samples. The XRD patterns displayed three principal peaks at 15.9°, 22.2°, and 34.6°, indicative of cellulose type I, which are typical crystal peaks of cellulose extracted from the RH. Notably, the broadening of the peak at 22.2° of the NCCs particles clearly indicates the nanocrystalline features of the NCCs particles and its strong intensity suggests the proportionality of crystalline structure. Additionally, the extracted cellulose exhibits the cellulose Iβ crystalline form over the Iα type. Accordingly, it is considered that the NCCs extracted from the RH has a 1β crystalline type . The crystallinity index (CI) and average crystallite size of the sample was 47.44% and 1.3376 nm, respectively.

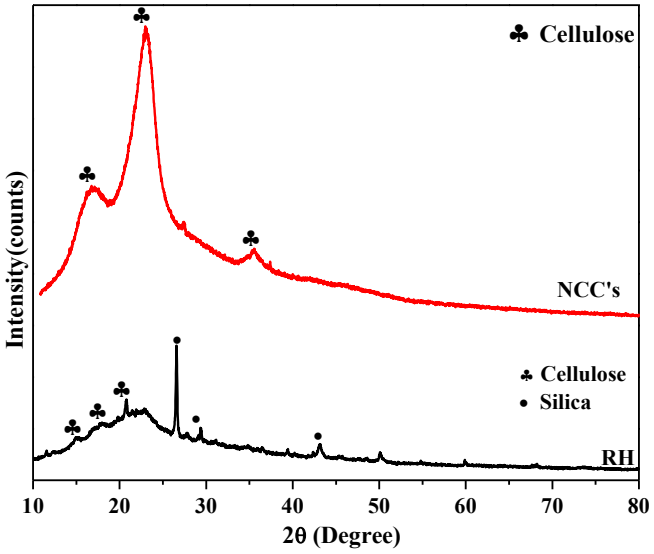


Fig. 5. XRD spectra of the as-received RH and the RH derived NCCs particles.

The porosity and specific surface area of NCC's were analyzed by using nitrogen adsorption isotherms and the results are displayed in **Fig. 6**. According to the IUPAC classification, the NCCs exhibits a type IV hysteresis isotherm, indicative of adsorption on mesoporous materials with significant adsorbate-adsorbent interactions. The type of isotherm is confirmed with linearity from 0.05 to 0.3 and a loop typically observed from 0.4 to 0.9 , . From the isotherm data, the NCCs were determined to have a specific surface area of 6.63 m^2/g and a total specific pore volume of 0.0241 cm^3/g. In addition, these NCCs has a density of 0.808 g/cm^3 and an average pore size of 16.93 nm. The porous nature of NCCs provides a large surface area for the loading of CP particles, which may be assumed to be embedded within the porous as well as to the partial inclusion of CP molecules within the nano cavities. The NCCs has a surface area of 3.727 m^2/g as measured by the BET surface area analyzer.

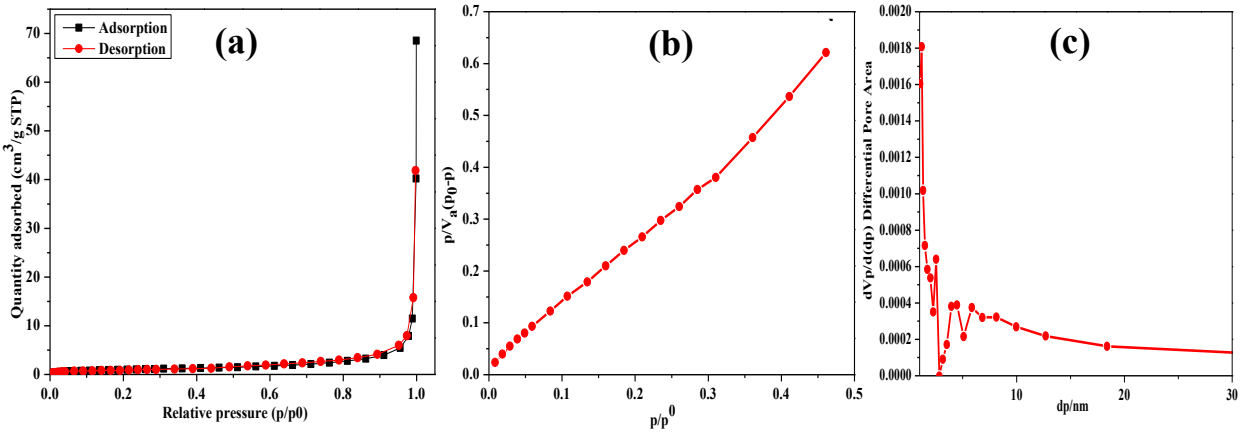


Fig. 6. (a) N_2 adsorption-desorption isotherms, (b) BET graph, and (c) BJH graph.

3.2 Drug loading efficiency of the NCCs

The amount of drug loading was determined by using a UV-Vis spectrometer with solvent evaporation technique. Calibration curve was obtained for CP at room temperature in ethanol: DCM solution. A fixed proportion of NCCs was dissolved to saturated drug solution and keep for continuous stirring for 24 h at 400 rpm. After 24 h, the resulting solution was centrifuged at 10000 rpm, and the supernatant was collected. The drug loading was determined by analyzing the supernatant by using a UV-Vis spectrometer at 263 nm, employing a calibration curve of CP with concentrations ranging from 10 to 50 µg/ml ($y = 0.01x + 0.014$ and $R^2 = 0.999$) as depicted in **Fig. 7(a)**. The drug loading amount was calculated by subtracting the remaining drug quantity in the supernatants from the initially used total drug amount. The maximum CP loaded per gram of NCCs carrier was approximately 200 µg/g.

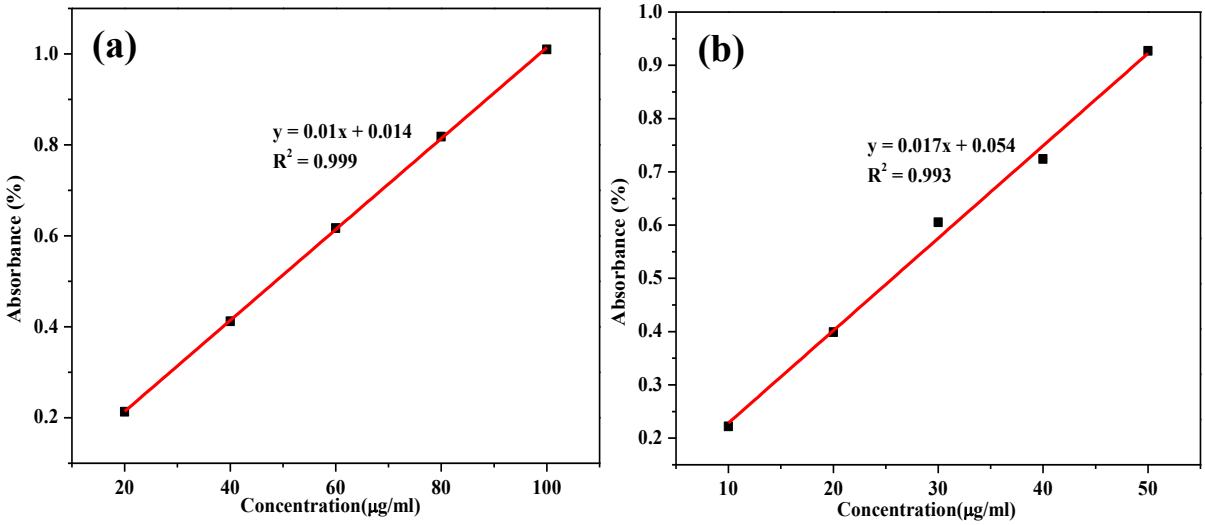


Fig. 7. (a) Calibration curve for measuring drug loading efficiency, and (b) calibration curve for evaluating drug releasing percentage in the PBS.

3.2.1 Structural analysis of the CP-NCCs

FTIR spectra of the CP, NCCs and CP-NCCs are shown in **Fig. 8**. FTIR spectra of CP exhibited characteristic peaks at 3400-3200 cm^{-1} for alcohol/phenol and peak at 1760 cm^{-1} corresponds to the ester carbonyl group. Peaks between 1450 and1375 cm^{-1} belong to the CH_3 group of alkane group. The out of plane bending for C-H group in alkene is observed in the range of 1000-650 cm^{-1}. Some of the prominent peaks evident in the FTIR spectra of CP-NCCs includes N-H stretch in the range of 3500-3100 cm^{-1}, ester carbonyl group at 1760 cm^{-1} and C-H out of plane bending in the range of

1000-650 cm^{-1} . It is also observed that there is a small shifting of peaks around 1461 cm^{-1} to 1451 cm^{-1} in the CP spectra after loading in NCCs . This shifting of peaks towards lower wavelength i.e. a red shift due to stretching of CH_3 group, shows a weak Van-der-walls force interaction between the NCCs and CP particles confirming the non-inclusion complex formation. Some others shift in the spectra from 1151 cm^{-1} to 1160 cm^{-1}, 1618 cm^{-1} to 1630 cm^{-1} and 2936 cm^{-1}, 2982 cm^{-1} to 2925 cm^{-1} and 2993 cm^{-1} showing CH_2 group twisting are also observed . Some peaks display a decrease in their intensity and some peaks' intensity increases after making complex with the NCCs. The peaks at 981 cm^{-1} and 953 cm^{-1} are merged and a small new peak around 987 cm^{-1} is appeared.

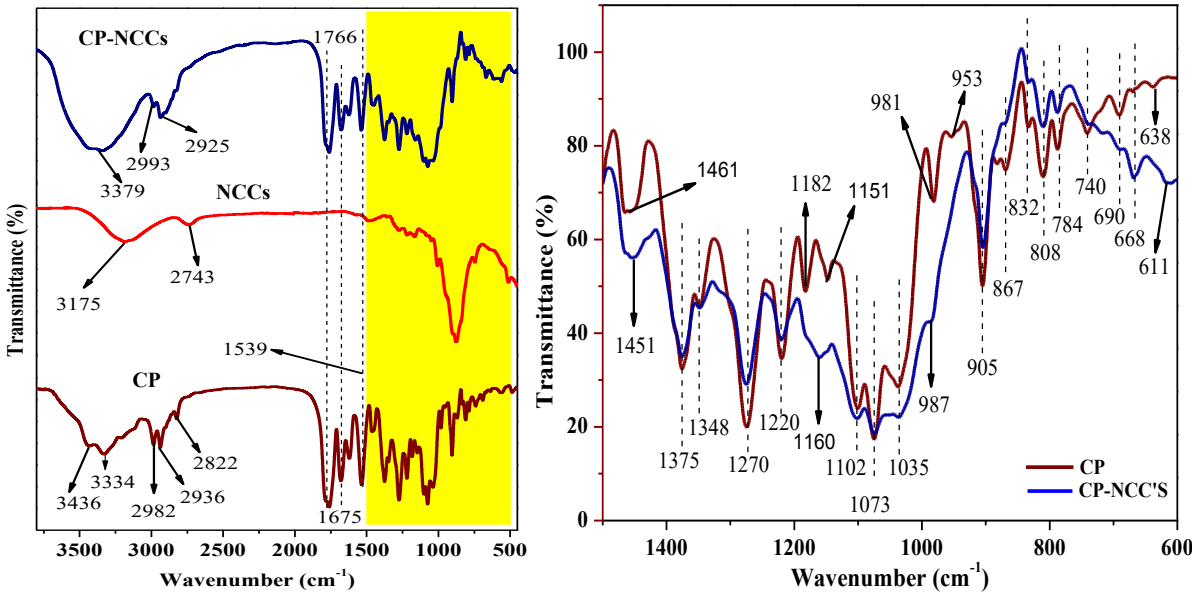


Fig. 8. FTIR spectra of CP, NCCs, and CP-NCCs samples.

3.2.2 In vitro dissolution study of the CP-NCCs

To evaluate the efficiency of NCCs as nano-drug carriers, a release profile analysis was conducted by using the CP. The analysis is depicted in **Fig. 9**, which shows the drug release profile of CP-NCCs in a pH 1.2 environment at 37 °C. In the study, a specified quantity of CP-NCCs was immersed in 50 ml of PBS solution at pH 1.2 and maintained at 37 °C, while being continuously shaken. At predetermined intervals, 2 ml samples were extracted from the solution, and the released amount of CP was measured using UV-Vis spectrometry. In addition, a calibration curve for pH 1.2 was created to ascertain the quantity of CP released, as illustrated in **Fig. 7(b)**. *In vitro* dissolution studies in the PBS show a release of 4.47% in starting 30 minutes, which was continuously increasing with time and exhibit a release of 99% in 10 h. A rapid drug release was found in starting 60 min, but constant release was achieved from 2 h to 4 h. After 4 h the drug

again shows a rapid release till 10 h. The dissolution pattern of CP in the PBS presents a rapid dissolution in the starting time. This might be because in the starting time the drug particles had the maximum surface area exposed to the solvent, leading to a rapid dissolution. After 8% dissolution, the drug dissolution shows slow release, which is almost constant till 20% dissolution. It might be due to the increase in the concentration of the drug in solvent to near saturation. The rate of dissolution is slowed down as the chemical potential driving dissolution has decreased.

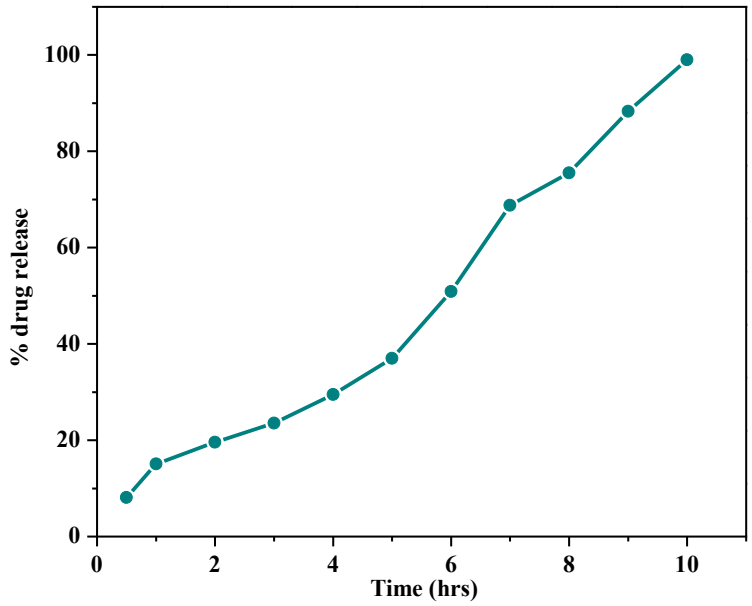


Fig. 9. Drug release profile of the CP-NCCs in the PBS media at different time intervals.

To study the release kinetics, the data obtained from *in vitro* drug release studies are plotted in the various kinetic models: zero order as cumulative amount of % drug released vs. time, first order as log cumulative percentage of drug remaining vs. time, Higuchi's model as cumulative percentage of drug released vs. square root of time, and Korsmeyer-Peppas model as log % of drug released vs. log time per hours, as depicted in **Fig.10**. The zero order rate constant as displayed in **Fig. 10(a)** shows the drug eliminated from the body regardless of its concentration. A value of 7.13 means the drug was eliminated at a rate of 7.13 mg/L per unit time and R^2 value indicates that 91% of the variability in the data could be explained by the zero-order model, suggesting a strong fit. The first order (**Fig. 10(b)**) reveals the release rate being dependent on concentration. Compared to the Zero order model, the first order model with $K_1 = 0.20$ and $R^2 = 0.60$ appeared to be a less fit. A value of 0.20 indicated a relatively slow elimination rate constant; this means that the drug was eliminated at a rate of 20% of its concentration per unit time. The Higuchi square root kinetics showing the

cumulative percent drug release vs. the square root of time (**Fig. 10(c)**), the high K_H value reflected a rapid dissolution from the formulation with a strong correlation ($R^2 = 0.81$). The high-rate constant described the high dissolution, which might impact its bioavailability. The log cumulative percent drug release vs. time for the Korsmeyer-Peppas indicates that the plot does not shows good linearity. The release rate constants and the regression coefficient values of the different models are summarized in **Table 1**.

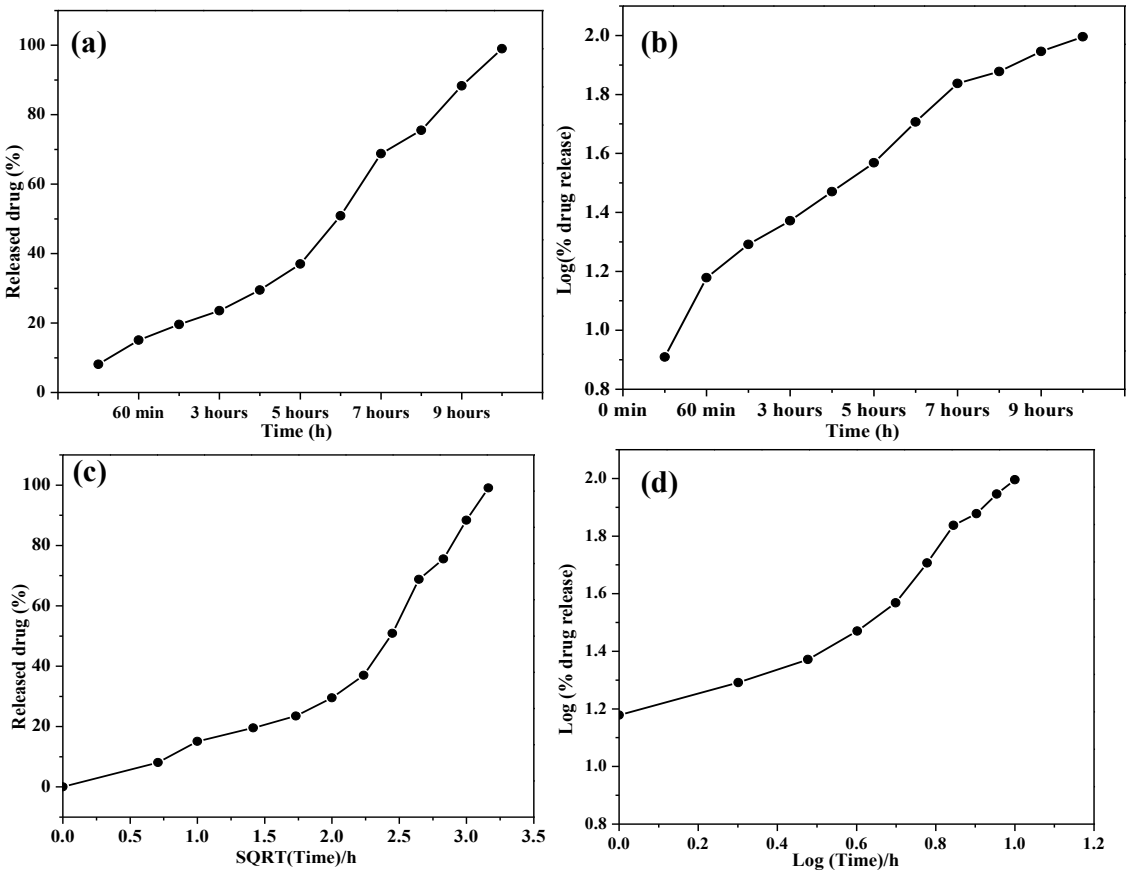


Fig. 10. Kinetics model for the release of CP from the CP-NCCs formulation: (a) zero-order, (b) first order, (c) Higuchi, and (d) Korsmeyer-Peppas model of kinetics.

Table 1. The release rate constant (K) and regression coefficient (R^2) values of the different models.

Formulation	pH	Zero-order		First-order		Higuchi model		Korsmeyer-Peppas	
		K_0	R^2	K_1	R^2	K_H	R^2	K	R^2
CP-NCCs	1.2	7.13	0.91	0.20	0.60	23.9	0.81	0.39	0.52

3.2.3 Molecular modeling of the CP and NCCs

The presence of an extensive hydrogen bonding within the nanocellulose crystals (NCCs) led to a tightly packed structure, leaving a little room for forming a cavity that could encapsulate another molecule. The CP is a relatively large and complex molecule with multiple functional groups, rings and side chains. Its bulky and irregular shape makes it difficult to fit into a cavity. From **Fig. 11**, we can see that the CP has a length of 10.986Å and width of 7.702Å as determined by using a mercury software [43]. This indicates that the molecular dimension and conformation of the molecules were such that the inclusion complex within the NCCs was not possible. The CP and NCCs could potentially interact via non-covalent bonds, primarily through hydrogen bonding and possibly some van-der-Waals forces. It is therefore important to note that these were not strong covalent bonds but rather weaker and more transient interactions that could play a role in pharmacokinetic processes or formulation characteristics in pharmaceuticals. The NCCs are composed of glucose units linked with β (1-4) glycosidic bonds. It is rich in hydroxyl groups (-OH) which can act as both hydrogen acceptors and donors. The ester group (-COO-) in the CP can act as hydrogen bond acceptor. When the CP is metabolized into its active form cefpodoxime, the ester is hydrolyzed, and the carboxyl group (COOH) that forms can act both as hydrogen donor and acceptor. Amide group present in the CP can also participate in hydrogen bonding; the amide nitrogen can be a hydrogen bond donor and amide oxygen act as acceptor of hydrogen bond. Due to larger surface area and polarizability, which enhance London dispersion forces. The CP and NCCs form van-der-Waals attraction. Furthermore, the complementary polar and non-polar regions of the CP and NCCs allow for multiple interaction sites, increasing the overall strength of these van-der-Waals forces. These interactions are critical for understanding for how the CP can interact with the cellulose, potentially impacting its release and bioavailability.

The BET data confirmed that the NCCs had large surface area and hence could interact with drug molecules via surface adsorption rather than inclusion within a cavity. Also, the FTIR data confirmed that the interaction between cellulose nanoparticles and the CP was van-der-Waals type interaction and not hydrogen bonding or any other type of bonding was present.

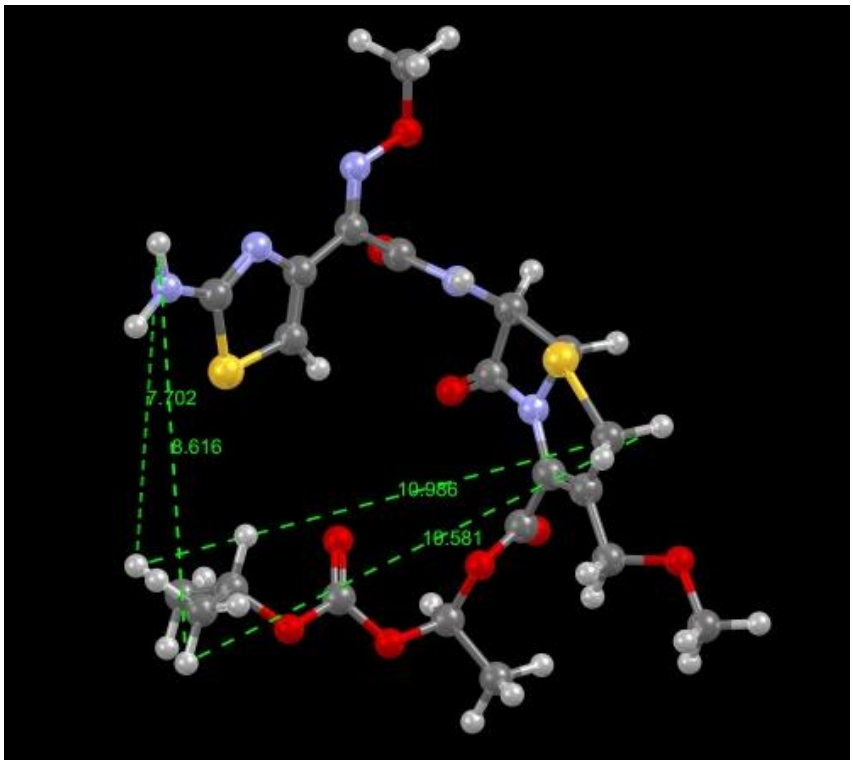


Fig. 11. Molecular modeling of the CP and NCCs by using a mercury software.

3.2.4 Antibacterial property of the CP-NCCs

The antibacterial property of the CP-NCCs was carried by measuring the zone of inhibition (ZOI) via disc diffusion test. The differences in the ZOI were measured with and without the NCCs. The values of ZOI for CP, NCCs and CP-NCCs were found to be 3 mm, 5 mm and 6 mm, respectively, with *E. coli*. No positive effects were obtained with *B. subtilis*. These findings indicate that the NCCs could serve as a potential carrier or enhancer for the CP. The complex of NCCs and CP exhibited the highest value of ZOI (i.e. 6 mm), demonstrating a synergistic effect between these two components (**Fig. 12**). This increase in efficacy could be attributed to the improved delivery or sustained release of CP when bound with the NCCs, allowing the antibiotic to remain in contact with bacterial cells for a longer period or at a higher local concentration. The interaction between the NCCs and CP may also enhance the penetration of the antibiotic into bacterial cells further boosting its antibacterial action.

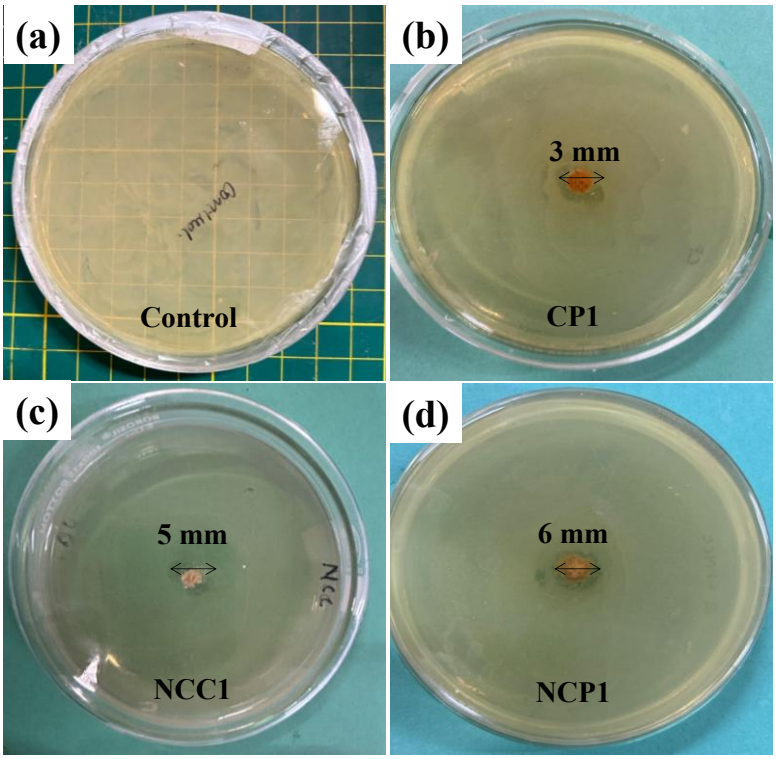


Fig. 12. Antibacterial testing for (a) control, (b) CP, (c) NCCs, and (d) drug loaded carrier against *E.coli*

4. Conclusions

In conclusion, nanocellulose crystals were extracted from the biowaste rice husk by a facile chemical synthesis route. The structural characterizations of the nanocellulose confirmed its nanometric size, high surface area, and the presence of functional groups is capable of facilitating drug loading. Thus, the cefpodoxime proxetil was incorporated into the nanocellulose matrix demonstrating a remarkable increase in the solubility of the drug. The *in vitro* release studies of cefpodoxime proxetil from the nanocellulose matrix indicated a sustained release profile. The drug loading efficiency and encapsulation efficiency were optimized through various formulation parameters, showcasing the versatility and adaptability of nanocellulose as a carrier system. These intrinsic properties of nanocellulose extracted from a biowaste source not only underscore the sustainability of this approach but also its potential in reducing environmental impact promoting a circular economy in pharmaceutical applications. While this research marks a significant step forward, it also opens avenues for further investigation. Future studies could explore the scalability of potential for tailoring the physicochemical properties of the nanocellulose-drug complex to achieve desired release profiles, offering a customizable platform for drug delivery applications.

Acknowledgements

Authors would like to acknowledge the contribution of IIT (BHU) for providing the necessary research facilities. Authors are also thankful to the Central Instrument Facility (CIF) at IIT (BHU) Varanasi for providing the characterization facilities for this work.

Author's contributions: Ms. Mukta Rajotia did formal literature review, experimental studies and analysis of data, prepared the original draft. Dr. Bechan Sharma reviewed and corrected the original draft. Dr. Sanjeev Kumar Mehto and Ms. Priya Singh helped in antibacterial testing and analysis. Dr. Subrata Panda supervised the work, edited and reviewed the final manuscript.

Declarations:

Conflicts of interest: No conflicts of interest

Ethical approval: Not applicable

Competing Interests: No known competing financial interest or personal relationships that could have appeared to influence the work reported in this paper

Funding: Not applicable

Availability of data and materials: Not applicable

References

[1] H. Xie, H. Du, and X. & Si, C. Yang, "Recent strategies in preparation of cellulose nanocrystals and cellulose nanofibrils derived from raw cellulose materials," *International Journal of Polymer Science*, 2018.

[2] I. & Plackett, D. Siró, "Microfibrillated cellulose and new nanocomposite materials: a review," *Cellulose*, vol. 17, pp. 459-494, 2010.

[3] S. & Dutta, H. Rashid, "Industrial applications of cellulose extracted from agricultural and food industry wastes," *Handbook of Biomass Valorization for Industrial Applications*, pp. 417-443, 2022.

[4] A. & Sain, M. Alemdar, "Isolation and characterization of nanofibers from agricultural residues–Wheat straw and soy hulls," *Bioresource technology*, vol. 99(6), pp. 1664-1671, 2008.

[5] N. Sathitsuksanoh and A. & Zhang, Y. H. P. George, "New lignocellulose pretreatments using cellulose solvents: a review," *Journal of Chemical Technology & Biotechnology*, vol. 88(2), pp. 169-180, 2013.

[6] U. & Anand, N. Tyagi, "Prospective of Waste Lignocellulosic Biomass as Precursors for the Production of Biochar: Application, Performance, and Mechanism—A Review," *BioEnergy Research*, pp. 1-26, 2023.

[7] R. Chandra and H. & Hasegawa, T. Takeuchi, "Methane production from lignocellulosic agricultural crop wastes: A review in context to second generation of biofuel production," *Renewable and Sustainable Energy Reviews*, vol. 16(3), pp. 1462-1476, 2012.

[8] Neto, T. S., CarvalhoJr, J. A., Veras, C. A. G., Alvarado, E. C., Gielow, R., Lincoln, E. N., ... & Santos, J. C. (2009). Biomass consumption and CO_2, CO and main hydrocarbon gas emissions in an Amazonian forest clearing fire. *Atmospheric Environment*, *43*(2), 438-446.

[9] M. Thakur, A. Sharma, V. Ahlawat, and M. & Goswami, S. Bhattacharya, "Process optimization for the production of cellulose nanocrystals from rice straw derived α-cellulose," *Materials Science for Energy Technologies*, vol. 3, pp. 328-334, 2020.

[10] A. Cabiac, E. Guillon, F. Chambon, C. Pinel, and F.& Essayem, N. Rataboul, "Cellulose reactivity and glycosidic bond cleavage in aqueous phase by catalytic and non catalytic transformations," *Applied Catalysis A: General*, vol. 402(1-2), pp. 1-10, 2011.

[11] Q. Lu, X. Yu, A. E. A. Yagoub, and H. & Zhou, C. Wahia, "Application and challenge of nanocellulose in the food industry," *Food Bioscience*, vol. 43, p. 101285, 2021.

[12] S. M. & Woods, H. J. Mukherjee, "X-ray and electron microscope studies of the degradation of cellulose by sulphuric acid," *Biochimica et biophysica acta*, vol. 10, pp. 499-511, 1953.

[13] J. & Adibkia, K. Shokri, "Application of cellulose and cellulose derivatives in pharmaceutical industries," *In Cellulose-medical, pharmaceutical and electronic applications*, 2013.

[14] Zhang, J., Luo, N., Zhang, X., Xu, L., Wu, J., Yu, J., ...& Zhang, J. (2016). All-cellulose nanocomposites reinforced with in situ retained cellulose nanocrystals during selective dissolution of cellulose in an ionic liquid. *ACS Sustainable Chemistry & Engineering*, *4*(8), 4417-4423.

[15] D. Klemm, B. Heublein, and H. P. & Bohn, A. Fink, "Cellulose: fascinating biopolymer and sustainable raw material," *Angewandte chemie international edition*, vol. 44(22), pp. 3358-3393, 2005.

[16] K. Songsurang and K. & Muangsin, N. Siraleartmukul, "Mucoadhesive drug carrier based on functional-modified cellulose as poorly water-soluble drug delivery system," *Journal of microencapsulation*, vol. 32(5), pp. 450-459, 2015.

[17] S. Zuppolini, A. Salama, I. Cruz-Maya, and V. & Borriello, A. Guarino, "Cellulose amphiphilic materials: Chemistry, process and applications," *cellulose*, vol. 14(2), p. 386, 2022.

[18] F. Xie and P. & Van den Mooter, G. Fardim, "Porous soluble dialdehyde cellulose beads: a new carrier for the formulation of poorly water-soluble drugs," *International Journal of Pharmaceutics*, vol. 615, p. 121491, 2022.

[19] S. Wan, Y. Sun, and X. & Tan, F. Qi, "Improved bioavailability of poorly water-soluble drug curcumin in cellulose acetate solid dispersion," *Aaps pharmscitech*, vol. 13, pp. 159-166, 2012.

[20] K. Yamamoto, M. Nakano, T. Arita, and Y. & Nakai, Y. Takayama, "Dissolution behavior and bioavailability of phenytoin from a ground mixture with microcrystalline cellulose," *Journal of Pharmaceutical Sciences*, vol. 65(10), pp. 1484-1488, 1976.

[21] N. S. Abbas, M. Amin, M. A. Hussain, K. J. Edgar, and M. N. & Tremel, W. Tahir, "Extended release and enhanced bioavailability of moxifloxacin conjugated with hydrophilic cellulose ethers," *Carbohydrate polymers*, vol. 136, pp. 1297-1306, 2016.

[22] A. K. Sharma, R. K. Keservani, S. C. Dadarwal, and Y. L. & Ramteke, S. Choudhary, "Formulation and in vitro characterization of cefpodoxime proxetil gastroretentive microballoons," *Journal of Faculty of Pharmacy, Tehran University of Medical Sciences*, vol. 19(1), p. 33, 2011.

[23] L. Huang, X. Chen, T. X. Nguyen, H. Tang, and L. & Yang, G. Zhang, "Nano-cellulose 3D-networks as controlled-release drug carriers," *Journal of Materials Chemistry B*, vol. 1(23), pp. 2976-2984, 2013.

[24] C. J. Wijaya, S. N., Soetaredjo, F. E. Saputra, J. N. Putro, C. X. Lin, and A.& Ismadji, S. Kurniawan, "Cellulose nanocrystals from passion fruit peels waste as antibiotic drug carrier," *Carbohydrate polymers*, vol. 175, pp. 370-376, 2017.

[25] K. & Agrawal, S. Chugh, "Cefpodoxime: pharmacokinetics and therapeutic uses," *The Indian Journal of Pediatrics*, vol. 70, pp. 227-231, 2003.

[26] Y. Pan, J. Wang, and P.& Xiao, H. Cai, "Dual-responsive IPN hydrogel based on sugarcane bagasse cellulose as drug carrier," *International journal of biological macromolecules*, vol. 118, pp. 132-140, 2018.

[27] A. Mujtaba and M. & Kohli, K. Ali, "Statistical optimization and characterization of pH-independent extended-release drug delivery of cefpodoxime proxetil using Box–Behnken design," *Chemical engineering research and design*, vol. 92(1), pp. 156-165, 2014.

[28] M. K. & Karthikeyan, M. Deepa, "Cefpodoxime Proxetil Floating Microspheres: Formulation and In VitroEvaluation: Formulation cefpodoxime proxetil floating microspheres," *Iranian journal of pharmaceutical sciences*, vol. 5(2), pp. 69-72, 2009.

[29] A. N. Karim and L. S. Jasim, "Synthesis and characterization of poly (CH/AA-co-AM) composite: Adsorption and thermodynamic studies of benzocaine on from aqueous solutions," *International Journal of Drug Delivery Technology*, vol. 9, no. 4, pp. 558-562, 2019.

[30] F. Khan, R. Katara, and S. Ramteke, "Enhancement of bioavailability of cefpodoxime proxetil using different polymeric microparticles," *AAPS PharmSciTech*, vol. 11, pp. 1368-1375, 2010.

[31] M. I. H. Mondal, M. S. Yeasmin, and M. S. Rahman, "Preparation of food grade carboxymethyl cellulose from corn husk agrowaste," *International Journal of Biological Macromolecules*, vol. 79, pp. 144-150, 2015.

[32] Pasaribu, K. M., Ilyas, S., Tamrin, T., Radecka, I., Swingler, S., Gupta, A., ...&Gea, S. (2023). Bioactive bacterial cellulose wound dressings for burns with collagen in-situ and chitosan ex-situ impregnation. *International Journal of Biological Macromolecules*, *230*, 123118.

[33] A. E., Özel, C., Özarslan, A. C. & Yücel, S. Karaca, "The simultaneous extraction of cellulose fiber and crystal biogenic silica from the same rice husk and evaluation in cellulose-based composite bioplastic films," *Polymer Composites*, vol. 43(10), pp. 6838-6853, 2022.

[34] S. & Meenakshisundaram, O. Kathiresan, "Effect of alkali treated and untreated cellulose fibers and human hair on FTIR and tensile properties for composite material applications," *SN Applied Sciences*, vol. 4(3), p. 74, 2022.

[35] Chen, H., Yu, Y., Zhong, T., Wu, Y., Li, Y., Wu, Z., &Fei, B. (2017). Effect of alkali treatment on microstructure and mechanical properties of individual bamboo fibers. *Cellulose*, *24*, 333-347.

[36] L. K. Lazzari, M. V. G. Zimmermann, D. Perondi, V. B. Zampieri, and A. J. & Santana, R. M. C. Zattera, "Production of carbon foams from rice husk," *Materials Research*, vol. 22, p. e20190427, 2019.

[37] A. E. Karaca, C. Özel, and A. C. & Yücel, S. Özarslan, "The simultaneous extraction of cellulose fiber and crystal biogenic silica from the same rice husk and evaluation in cellulose-based composite bioplastic films," *Polymer Composites*, vol. 43(10), pp. 6838-6853, 2022.

[38] M. & Noroozi, B. Dilamian, "Rice straw agri-waste for water pollutant adsorption: Relevant mesoporous super hydrophobic cellulose aerogel," *Carbohydrate polymers*, vol. 251, p. 117016, 2021.

[39] S. Tang, Q. Dong, and Z. & Miao, Z. D. Fang, "Complete recovery of cellulose from rice straw pretreated with ethylene glycol and aluminum chloride for enzymatic hydrolysis," *Bioresource technology*, vol. 284, pp. 98-104, 2019.

[40] M. R. Rao, A. N. Bajaj, and A. A. & Aghav, S. S. Pardeshi, "Investigation of nanoporous colloidal carrier for solubility enhancement of Cefpodoxime proxetil," *Journal of pharmacy research*, vol. 5(5), pp. 2496-2499, 2012.

[41] A. M. A. Adam, H. A. Saad, A. M. Alsuhaibani, and M. S.& Hegab, M. S. Refat, "Charge-transfer chemistry of azithromycin, the antibiotic used worldwide to treat the coronavirus disease (COVID-19). Part III: A green protocol for facile synthesis of complexes with TCNQ, DDQ, and TFQ acceptors," *Journal of Molecular Liquids*, vol. 335, p. 116250, 2021.

[42] S. Suganthi, P. Balu, V. Sathyanarayanamoorthi, V. Kannappan, and M. M. & Kumar, R. Kamil, "Structural analysis and investigation of molecular properties of Cefpodoxime acid, a third generation antibiotic," *Journal of Molecular Structure*, vol. 1108, pp. 1-15, 2016.

[43] Chambers JE, Migliorini F. MERCURY-a new software package for orbital integrations. InAAS/Division for *Planetary Sciences Meeting,* Vol. 29, pp. 27-06, 1997.